Hindawi Publishing Corporation
International Journal of Optics
Volume 2012, Article ID 689612, 7 pages
doi:10.1155/2012/689612

Research Article

Generation of Optical Vortex Arrays Using Single-Element Reversed-Wavefront Folding Interferometer

Brijesh Kumar Singh,[1] G. Singh,[2] P. Senthilkumaran,[1] and D. S. Mehta[2]

[1] *Department of Physics, Indian Institute of Technology Delhi, Hauz Khas, New Delhi 110016, India*
[2] *Laser Applications and Holography Laboratory, Instrument Design Development Centre, Indian Institute of Technology Delhi, Hauz Khas, New Delhi 110016, India*

Correspondence should be addressed to Brijesh Kumar Singh, brijeshsingh831@gmail.com

Received 15 April 2011; Revised 7 June 2011; Accepted 8 June 2011

Academic Editor: Shunichi Sato

Optical vortex arrays have been generated using simple, novel, and stable reversed-wavefront folding interferometer. Two new interferometric configurations were used for generating a variety of optical vortex lattices. In the first interferometric configuration one cube beam splitter (CBS) was used in one arm of Mach-Zehnder interferometer for splitting and combining the collimated beam, and one mirror of another arm is replaced by second CBS. At the output of interferometer, three-beam interference gives rise to optical vortex arrays. In second interferometric configuration, a divergent wavefront was made incident on a single CBS which splits and combines wavefronts leading to the generation of vortex arrays due to four-beam interference. It was found that the orientation and structure of the optical vortices can be stably controlled by means of changing the rotation angle of CBS.

1. Introduction

Optical vortices (OVs) are point phase defects, also called phase singularities in the distribution of optical wave-fields where both real and imaginary values of the optical fields are zero [1]. An interesting peculiarity of point phase defects is the helicoidal structure of the wave front around the defect axis and is described as $\exp(il\Phi)$, where l is the topological charge and Φ is the azimuthal angle around the defect axis. The magnitude of topological charge determines the degree of circulation, that is, the number of 2π cycles of phase accumulation around the vortex point. The sign of topological charge defines the handedness or helicity of the phase singular beam along the propagation direction of the z-axis. An interesting aspect of a vortex beam is that it possesses orbital angular momentum (OAM). Optical vortices play significant role for studying OAM of light fields [2, 3] and have been widely used in the area of optical tweezers [4], singular optics [5], optical solitons [6], and optical metrology [7, 8]. The most commonly used methods for generating OVs with single or multiple charge are synthetic holograms [9], spiral phase plates [10], liquid-crystal cells [11], dielectric wedge [12], and higher-order laser beams [13]. An alternative method for generating OVs efficiently is the use of optical fibers [14] such as, a hollow-core optical fiber for generating doughnut-shaped beam and a holey fiber for generating hollow beam.

Recently, there has been great interest for generating optical vortex arrays (OVAs) also called vortex lattices using multiple beam interference [15, 16]. It has been demonstrated that when three or more plane waves overlap in space, complete destructive interference occurs on nodal lines, also called phase singularities or optical vortices leading to the generation of regular net of vortex lattices. Various optical interferometric configurations have been implemented for generating vortex lattices. Generation of OVAs by three-, four- and five- plane wave interference [17], interferometric optical vortex array generator [18, 19], creation of OV lattices by wavefront division [20], using couple of Wollaston prisms [21, 22], and lateral shearing interferometers [23] have been reported. Such periodic arrays of optical vortices have been used as phase markers [22], in optical metrology for the measurements of small-angular rotations, tilt, orientation [24–26], and birefringence [27]. But most of the aforementioned interferometric techniques used for generating vortex lattices are based on modified Mach-Zehnder interferometer and multiple Michelson interferometers to generate and recombine three-, four-, or five-wave fronts. This requires the use of multiple beam-splitters, mirrors, attenuation plates, and vibration isolation table which makes the experimental setup complicated and demands tedious and precise alignment procedure. The existing systems for generating OVAs are bulky, expensive, and require alignment of multiple components and hence are not robust. The essential requirement of optical vortex interferometry is the generation of highly stable regular optical vortex lattice for improving the accuracy in measurement.

In this paper, we demonstrate the generation of optical vortex arrays using a novel reversed-wavefront folding interferometer. Multiple wavefronts are generated and combined by means of simple interferometric configurations. Similar situation of CBS was used earlier for measuring the degree of coherence [28], optical metrology [29], and digital holographic microscopy [30]. Two new interferometric configurations were used for generating a variety of vortex lattices. We demonstrate that the orientation and structure of the optical vortices can be stably controlled by means of changing the rotation angle of CBS. The main advantages of the present system are simple, robust, and inexpensive method for generating OVAs. The system can generate multiple wavefronts, interferograms, and one can change the orientation, structure, and spatial carrier frequency of OVAs by means of changing the angle of the CBS. The first interferometric configuration as shown in Figure 1(a) requires less vibration isolation table in comparison to second interferometric configuration (Figure 1(b)) and precise control, adjustment, and alignment of multiple optical components which are an essential requirement in the existing systems for generating OVAs [15–27].

2. Optical Vortex Array Generation

The schematic diagram of the modified Mach-Zehnder interferometer by two CBSs for generating optical vortex lattices using collimated beam is shown in Figure 1(a). Gaussian beam (TEM_{00} fundamental mode) from a CW green laser having power 30 mW and wavelength $\lambda = 532$ nm was expanded and spatially filtered. A collimated beam is then made to incident onto a 50/50 CBS_1 (size 50 mm × 50 mm). Two CBSs are used to modify the Mach-Zehnder interferometer. CBS_2 is used in first arm, while the CBS_3 is used to replace the mirror in second arm of the interferometer. The transmitted wavefront in the first (upper) arm of the interferometer is divided into two parts called input 1 and input 2. When input 1 is incident on the CBS_2, it will be reflected and transmitted through semireflecting layer. Reflected part will be the reverted replica of the input 1, and it will get an extra phase shift of $\pi/2$ (rad). The transmitted part will be the translated replica of the input 1. Similarly when input 2 is incident on CBS_2 two replicas of itself at the output of the CBS_2 will be available. Hence at one of the outputs of the CBS_2 reflected replica of input 1 and transmitted replica of input 2 will interfere with each other and generate interference fringe pattern 1 (IFP1). Similarly interference of reflected replica of input 2 and transmitted replica of input 1 will generate interference fringe pattern 2 (IFP2) at the other output of CBS_2 as shown in Figure 1(a). The ray diagram for the input 1 and 2 in the CBS_2 is shown in the left bottom of Figure 1(a). A detailed analysis of generating two interferograms using single CBS in presence of collimated beam is given in [29]. The rotation of the CBS_2 is also shown. The CBS_2 rotates about the x-axis which is normal to the paper, and angle θ is measured between z-axis (propagation direction of the incident beam) and semireflecting plane of the CBS_2. As the angle θ is increased, both the orientation and number of straight line fringes of IFP 1 and 2 increase.

In the case of collimated beam, both IFP 1 and IFP 2 propagate parallel to each other and will not overlap. Both IFP 1 and 2 propagate in space and reflected by mirror M_1 and again transmitted through CBS_4. The beam input 3 in the second (lower) arm of the interferometer is reflected by CBS_3 and after propagation in space again reflected by CBS_4 where it interferes with IFP 1 and IFP 2 at the output. At the end of the interferometer, optical vortex arrays are generated by interference of three beams. Two beams come from first arm and one beam comes from second arm of the modified Mach-Zehnder interferometer. CBS_3 is used to make the amplitude of the interference beam equal for vortex lattices generation. Interference of beam input 3 with IFP 1 and 2 generate the optical vortex arrays 1 (OVAs 1) and OVAs 2 at the output of the interferometer as shown in Figure 1(a).

Second configuration for generating the vortex lattices by using a single CBS is shown schematically in Figure 1(b). Gaussian beam (TEM_{00} fundamental mode) from a CW green laser having power 30 mW and wavelength $\lambda = 532$ nm was expanded and spatially filtered (BE/SF) and a divergent beam was then made incident on to the 50/50 CBS (size 50 mm × 50 mm). The CBS was kept in unconventional position so as to both split and combine the diverging spherical wave fronts [29, 30]. A light beam having spherical wave front (diameter 20 mm) traveling along the z-axis was made incident on the CBS with its central semireflecting layer placed along the propagation direction. The wavefront is divided into two parts called input 1 and input 2, and each beam generates two respective replicas of itself. The input beam 1 incident on the top front cube wall changes the direction of propagation inside the CBS and is divided into two parts, first is reflected and second is transmitted and finally exit from the CBS as shown in Figure 1(b). Because of the reflection that occurs at the internal semireflecting surface of the CBS, one of the two replicas will acquire an extra phase-shift of $\pi/2$ (rad), as required by symmetry and energy conservations [29]. Similarly, the other beam input 2 incident on the bottom front cube wall generates two replicas of the beam, one transmitted and other reflected with an extra phase-shift of $\pi/2$ (rad). The two spherical beams generated by transmission through the beam-splitter will be simply translated replicas of the input fields, while the reflected beams will be translated and reverted replicas. In this way, there are four diverging spherical beams at the output of the CBS. Two output beams exiting on the top of CBS generate interference fringe pattern 1 (IFP 1), and the two beams exiting at the bottom generate interference fringe pattern 2 (IFP 2). As it is a common-path interferometer, all

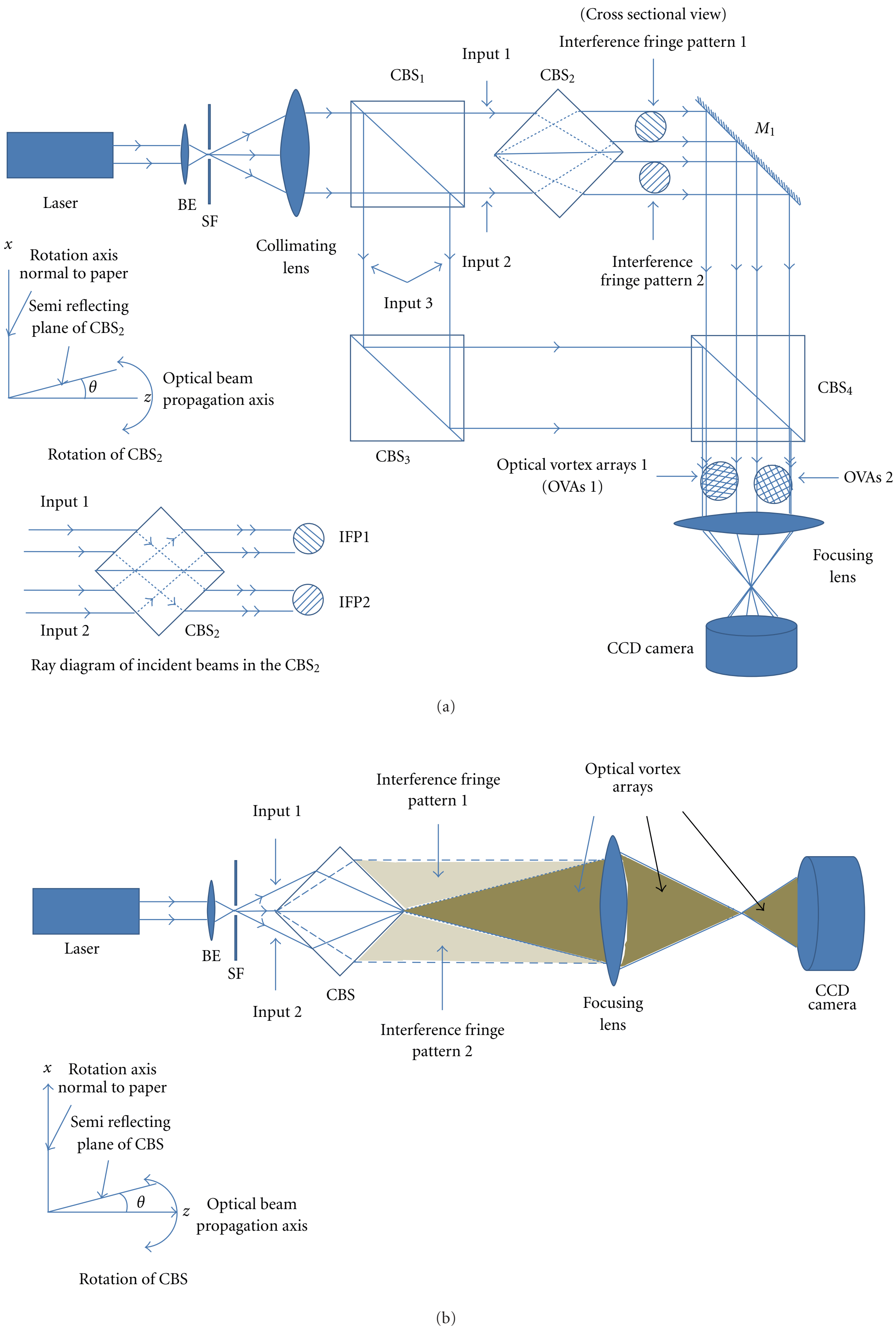

Figure 1: Schematic diagrams for generating optical vortex arrays: (a) by using collimated beams in modified Mach-Zehnder interferometer; (b) by using spherical wavefronts in single element common path interferometer. BE: beam expander, SF: spatial filter, CBS: cubic beam splitter, CCD: charge-coupled device, IFP: interference fringe pattern.

the four beams generated by input 1 and 2 travel the same distance and the interference fringes can be obtained. The CBS was mounted on a rotating table, and a small angle θ was introduced between the light propagation direction and the central semireflecting layer (Figure 1(b)). Due to this, a wedge-shaped optical path difference is introduced to the reflected light and the transmitted light which results in interferograms with straight line fringes. The rotation axis and the orientation of CBS are the same as for the CBS_2 in Figure 1(a). The orientation of fringes in IFP 1 and IFP 2 is opposite to each other (Figure 1(b)). If the orientation angle of the IFP 1 is changed, orientation angle of the IFP 2 will also change accordingly. The orientation and the spatial carrier frequency of the IFP 1 and 2 can be easily controlled by means of changing angle θ [29, 30]. The two interferograms IFP 1 and 2 are highly diverging and as the distance of propagation increases they start overlapping to each other. In the region of overlap, they produce optical vortex arrays due to destructive interference among the four spherical waves. In Figure 1(a), we used the collimated beam while in Figure 1(b) diverging beam is used. In both cases (in Figures 1(a) and 1(b)), a focusing lens was used to reduce the size of the beams so that both the output interference patterns can be recorded using a single CCD camera. The main advantages of the proposed setup are its simplicity and insensitive to vibration, and hence the interferometer generates stable optical vortex lattices.

2.1. Reconstruction of Phase Map. This interference due to the superposition of three plane waves $a_1 e^{i2\pi(f_{1x}x+f_{1y}y)}$, $a_2 e^{i2\pi(f_{2x}x+f_{2y}y)}$, and $a_3 e^{i2\pi(f_{3x}x+f_{3y}y)}$ gives rise to a two-dimensional fringe pattern that contains vortices. The superposition of above three-plane waves can be written as

$$\begin{aligned} &a_1(x,y)e^{i2\pi(f_{1x}x + f_{1y}y)} + a_2(x,y)e^{i2\pi(f_{2x}x + f_{2y}y)} \\ &\quad + a_3(x,y)e^{i2\pi(f_{3x}x + f_{3y}y)} = b(x,y)e^{i\varphi}. \end{aligned} \tag{1}$$

And the interference intensity distribution is

$$\begin{aligned} g(x,y) &= a_1^2(x,y) + a_2^2(x,y) + a_3^2(x,y) \\ &\quad + 2a_1(x,y)a_2(x,y) \\ &\quad \times \cos\left[2\pi\left((f_{1x} - f_{2x})x + \left(f_{1y} - f_{2y}\right)y\right)\right] \\ &\quad + 2a_2(x,y)a_3(x,y) \\ &\quad \times \cos\left[2\pi\left((f_{2x} - f_{3x})x + \left(f_{2y} - f_{3y}\right)y\right)\right] \\ &\quad + 2a_1(x,y)a_3(x,y) \\ &\quad \times \cos\left[2\pi\left((f_{1x} - f_{3x})x + \left(f_{1y} - f_{3y}\right)y\right)\right]. \end{aligned} \tag{2}$$

For convenience, we write

$$\begin{aligned} g(x,y) = b^2 &= a_1^2(x,y) + a_2^2(x,y) + a_3^2(x,y) \\ &\quad + 2a_1(x,y)a_2(x,y)\cos(\theta_1 - \theta_2) \\ &\quad + 2a_2(x,y)a_3(x,y)\cos(\theta_2 - \theta_3) \\ &\quad + 2a_1(x,y)a_3(x,y)\cos(\theta_1 - \theta_3). \end{aligned} \tag{3}$$

Equation (3) can be written in generalized form as

$$g(x,y) = \sum_{j=1}^{3} a_j^2(x,y) + 2\sum_{j=1}^{3}\sum_{k>j}^{3} a_{jk}(x,y)\cos\left(\Delta\theta_{jk}(x,y)\right), \tag{4}$$

where $a_j^2(x,y)$ and $a_{jk}(x,y) = a_j a_k$ (for $j,k = 1,2,3$) are the background intensity and fringe amplitude for the three-beam interference. $\Delta\theta_{jk} = \theta_j - \theta_k$, $\theta_j = 2\pi(f_{jx}x + f_{jy}y)$ and $\theta_k = 2\pi(f_{kx}x + f_{ky}y)$, where $f_{jx}, f_{kx}, f_{jy}, f_{ky}$ (for $j,k = 1,2,3$) are the spatial frequency of the first, second, and third beam in the x and y directions, respectively.

The Fourier transform of the intensity distribution is consisting of nine spots, further

$$\begin{aligned} \mathcal{F}\{b^2(x,y)\} &= \mathcal{F}\left\{b(x,y)e^{i\varnothing}\right\} \otimes \mathcal{F}\left\{b(x,y)e^{-i\varnothing}\right\} \\ &= \left\{A_1\left(f_x, f_y\right) \otimes \delta\left(f_x - f_{1x}, f_y - f_{1y}\right)\right. \\ &\quad + A_2\left(f_x, f_y\right) \otimes \delta\left(f_x - f_{2x}, f_y - f_{2y}\right) \\ &\quad \left. + A_3\left(f_x, f_y\right) \otimes \delta\left(f_x - f_{3x}, f_y - f_{3y}\right)\right\} \\ &\quad \otimes \left\{A_1^*\left(f_x, f_y\right) \otimes \delta\left(f_x + f_{1x}, f_y + f_{1y}\right)\right. \\ &\quad + A_2^*\left(f_x, f_y\right) \otimes \delta\left(f_x + f_{2x}, f_y + f_{2y}\right) \\ &\quad \left. + A_3^*\left(f_x, f_y\right) \otimes \delta\left(f_x + f_{3x}, f_y + f_{3y}\right)\right\}, \end{aligned} \tag{5}$$

where $A_j(f_x, f_y) = \mathcal{F}\{a_j(x,y)\}$, for $j = 1,2,3$. This can be seen from (3) by writing $\cos(\Delta\theta) = (1/2)[e^{i\Delta\theta} + e^{-i\Delta\theta}]$ and noting that the FT consists of 3δ functions overlapping at the origin and six δ functions at the locations given by $f_x, f_y = f_{jx} \mp f_{kx}, f_{jy} \mp f_{ky}$ ($k > j$, $j,k = 1,2,3$).

By selecting three of the δ functions (at $(f_{1x} - f_{2x}, f_{1y} - f_{2y})$, $(f_{2x} - f_{3x}, f_{2y} - f_{3y})$, $(f_{1x} - f_{3x}, f_{1y} - f_{3y})$), and taking inverse Fourier transform (IFT), the phase distribution of the intensity modulated fringes can be obtained. This phase distribution can be extracted by separating out the imaginary part of the logarithm complex function obtained by IFT operation.

This is actually the phase distribution corresponding to

$$\begin{aligned} &2a_1(x,y)a_2(x,y)\cos(\theta_1 - \theta_2) \\ &\quad + 2a_2(x,y)a_3(x,y)\cos(\theta_2 - \theta_3) \\ &\quad + 2a_1(x,y)a_3(x,y)\cos(\theta_1 - \theta_3), \end{aligned} \tag{6}$$

which are the modulation terms in the intensity pattern.

3. Experimental Results

Figure 2 is the interference pattern obtained from the experimental setup shown in Figure 1(a) in which we record the formation of optical vortex arrays (OVAs) using the interference of three plane waves. At the exit of CBS_4 as shown in the Figure 1(a), we obtain two optical vortex arrays

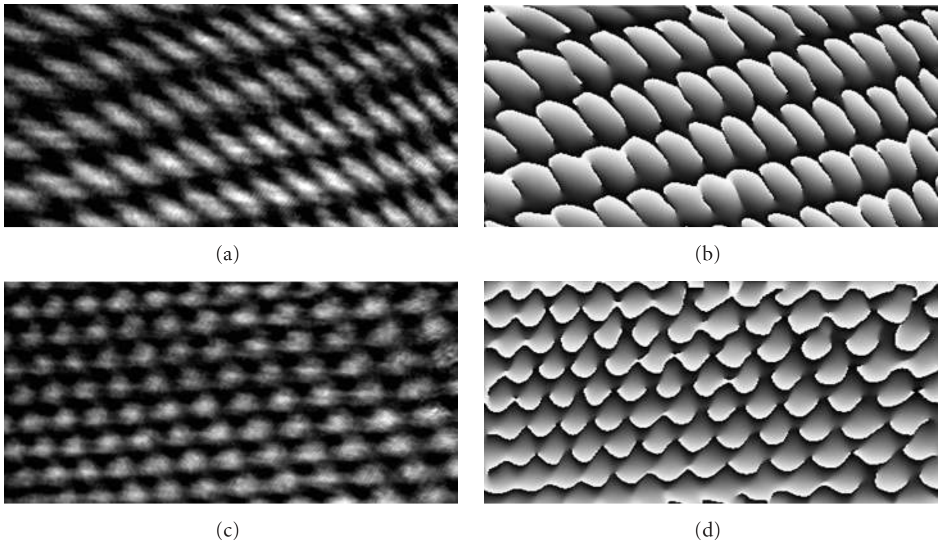

(a) (b) (c) (d)

Figure 2: (a) and (c) are the recorded interferograms of generated vortex arrays at the rotation angles 0.25° and 0.30° of CBS_2 by using experimental set-up Figure 1(a) and (b) and (d) are the corresponding phase-maps due to the superposition of three plane wavefronts respectively.

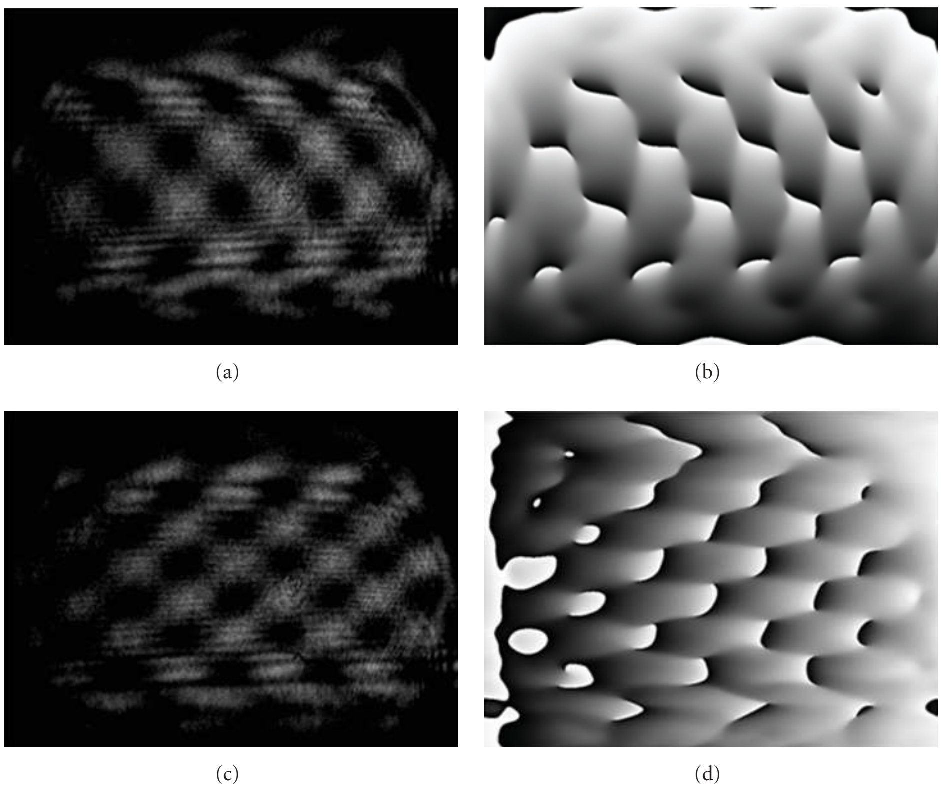

(a) (b) (c) (d)

Figure 3: (a) and (c) are the recorded interferograms of generated vortex arrays at the rotation angles 0.25° and 0.40° of CBS by using experimental set-up Figure 1(b) and (b) and (d) are the corresponding phase-maps due to the superposition of four spherical wavefronts respectively.

(OVAs 1 and OVAs 2) side-by-side in the transverse plane. The generation of OVAs are due to the interference of three beams in which two beams are coming from first (upper) arm while third beam is coming from second (lower) arm of the interferometer. Figures 2(a) and 2(c) show the recorded interferogram of three beam interference where the OVAs is present while Figures 2(b) and 2(d) show the phase-map corresponding to Figures 2(a) and 2(c), respectively.

First, we put the CBS_2 in the experimental setup (Figure 1(a)) in this way that the transmitted beam from CBS_1 and the central line of CBS_2 are nearly parallel to each other. The CBS_2 was then rotated around an axis which is normal to the optical table and optical axis, in either direction with the rotation angle incremented by $\sim 0.05^\circ$. On increasing the rotation angle θ with a step of $\sim 0.05^\circ$, both the orientation as well as the spatial carrier frequency of the individual interferograms (IFP 1 and IFP 2) increase by equal amount. The orientation of the fringes is opposite in the two fields IFP 1 and IFP 2. By interfering these fringes with third plane beam coming from lower arm of the interferometer, a perfectly knitted pattern of vortex lattices was observed as can be seen from Figures 2(a) and 2(c). Another point is that in the present setup a variety of vortex lattices can be generated by means of changing the small rotation angle of $CBS_{2..}$. The density of the optical vortices was further increased on increasing the rotation angle of the CBS_2 as can be seen from Figure 2(c). It can also be seen from Figures 2(a) and 2(c) that dark spots appear in the overlap region, and in each dark spot a phase dislocation is present. This can be seen from the constructed phase maps (Figures 2(b) and 2(d)). The vortex lattice generation using the collimated beam (Figure 1(a)) is similar to the generation of vortex lattices by four or more plane waves as has been demonstrated previously using multiple beam interferometers [15–17].

Figures 3(a) and 3(c) show the recorded interferograms using divergent beam in the experimental setup as shown in Figure 1(b). A divergent beam incident on a CBS gives two interferograms (IFP 1 and IFP 2) side-by-side as shown in Figure 1(b). They overlap as the distance of propagation increases as shown in Figure 1(b). When the central line of CBS is perfectly parallel to optical axis, the fringes in both the interferograms IFP 1 and IFP 2 are vertical straight lines in the overlap region. As shown in Figure 1(b), the CBS was then rotated around an axis which is normal to the optical table and optical axis, in either direction with the rotation angle incremented by $\sim 0.05^\circ$. On increasing the rotation angle θ with a step of $\sim 0.05^\circ$ both the orientation as well as the spatial carrier frequency of the individual interferograms (IFP 1 and IFP 2) increases with equal amount and the orientation of the fringes is in the opposite direction. In the region where all the four beams overlap, optical vortices are generated. It is visible from Figures 3(a) and 3(c) that dark spots appear in the overlap region, and corresponding to each dark spot phase dislocations can be seen from the corresponding phase map as shown in Figures 3(b) and 3(d), respectively. The density of optical vortices was further increased on increasing the rotation angle of the CBS as can be seen from Figure 3(c). Extraction of the phase distributions from the interferograms is done by Fourier transform fringe analysis method [31]. So in this way, the vortex arrays can be generated using a stable single element optical interferometer as shown in Figure 1(b). The orientation and the spatial-carrier frequency can be easily controlled by simply changing the rotation angle of the CBS. The main advantage of the present system is that the vortex lattices are stable due to the common path interferometer. This kind of setup is highly useful for multiple trapping of microparticles and biological cells in the optical tweezers.

4. Conclusions

In conclusion, we have demonstrated an efficient, simple, and cost-effective method for generating optical vortex arrays using simple and highly stable reversed-wavefront folding interferometer. Two new interferometric configurations have been used for generating a variety of vortex lattices. In the first interferometric configuration, two CBSs were then used to modify the Mach-Zehnder interferometer and then by interference of three beams optical vortex arrays are generated. In second configuration, a divergent wavefront was made incident on a single CBS which splits and combines wavefronts leading to the generation of vortex arrays due to four-beam interference. It was found that the orientation and structure of the optical vortices can be stably controlled by means of changing the rotation angle of CBS. Further, the spatial-carrier frequency and the orientation of the interference fringes can be stably controlled. The present systems have potential applications in multiple trapping and optical metrology. The most important advantages of the proposed setups for generating vortex lattices are their simplicity, minimal number of optical elements, and insensitivity to external vibrations.

Acknowledgment

B. K. Singh thankfully acknowledges University Grant Commission (UGC) of India for junior research fellowship.

References

[1] J. F. Nye and M. V. Berry, "Dislocation in wave trains," *Proceedings of the Royal Society A*, vol. 336, pp. 165–190, 1974.
[2] L. Allen, M. J. Padgett, and M. Babiker, "IV The orbital angular momentum of light," *Progress in Optics*, vol. 39, pp. 291–372, 1999.
[3] C.-S. Guo, S.-J. Yue, and G.-X. Wei, "Measuring the orbital angular momentum of optical vortices using a multipinhole plate," *Applied Physics Letters*, vol. 94, no. 23, Article ID 231104, 3 pages, 2009.
[4] K. T. Gahagan and G. A. Swartzlander Jr., "Optical vortex trapping of particles," *Optics Letters*, vol. 21, no. 11, pp. 827–829, 1996.
[5] M. S. Soskin, V. N. Gorshkov, M. V. Vasnetsov, J. T. Malos, and N. R. Heckenberg, "Topological charge and angular momentum of light beams carrying optical vortices," *Physical Review A*, vol. 56, no. 5, pp. 4064–4075, 1997.
[6] C. T. Law and G. A. Swartzlander, "Optical vortex solitons and the stability of dark soliton stripes," *Optics Letters*, vol. 18, no. 8, pp. 586–588, 1993.
[7] W. Wang, T. Yokozeki, R. Ishijima et al., "Optical vortex metrology for nanometric speckle displacement measurement," *Optics Express*, vol. 14, no. 1, pp. 120–127, 2006.
[8] W. Wang, T. Yokozeki, R. Ishijima, M. Takeda, and S. G. Hanson, "Optical vortex metrology based on the core structures of phase singularities in Laguerre-Gauss transform of a speckle pattern," *Optics Express*, vol. 14, no. 22, pp. 10195–10206, 2006.

[9] N. R. Heckenberg, R. McDuff, C. P. Smith, and A. G. White, "Generation of optical phase singularities by computer-generated holograms," *Optics Letters*, pp. 221–223, 1992.

[10] K. J. Moh, X.-C. Yuan, W. C. Cheong et al., "High-power efficient multiple optical vortices in a single beam generated by a kinoform-type spiral phase plate," *Applied Optics*, vol. 45, no. 6, pp. 1153–1161, 2006.

[11] D. Ganic, X. Gan, M. Gu et al., "Generation of doughnut laser beams by use of a liquid-crystal cell with a conversion efficiency near 100%," *Optics Letters*, vol. 27, no. 15, pp. 1351–1353, 2002.

[12] Y. Izdebskaya, V. Shvedov, and A. Volyar, "Generation of higher-order optical vortices by a dielectric wedge," *Optics Letters*, vol. 30, no. 18, pp. 2472–2474, 2005.

[13] C. Tamm and C. O. Weiss, "Bistability and optical switching of spatial patterns in a laser," *Journal of the Optical Society of America B*, vol. 7, pp. 1034–1038, 1990.

[14] R. Kumar, D. Singh Mehta, A. Sachdeva, A. Garg, P. Senthilkumaran, and C. Shakher, "Generation and detection of optical vortices using all fiber-optic system," *Optics Communications*, vol. 281, no. 13, pp. 3414–3420, 2008.

[15] J. Masajada and B. Dubik, "Optical vortex generation by three plane wave interference," *Optics Communications*, vol. 198, no. 1–3, pp. 21–27, 2001.

[16] J. Masajada, A. Popiołek-Masajada, E. Frączek, and W. Frączek, "Vortex points localization problem in optical vortices interferometry," *Optics Communications*, vol. 234, no. 1–6, pp. 23–28, 2004.

[17] K. O'Holleran, M. J. Padgett, and M. R. Dennis, "Topology of optical vortex lines formed by the interference of three, four, and five plane waves," *Optics Express*, vol. 14, no. 7, pp. 3039–3044, 2006.

[18] S. Vyas and P. Senthilkumaran, "Interferometric optical vortex array generator," *Applied Optics*, vol. 46, no. 15, pp. 2893–2898, 2007.

[19] S. Vyas and P. Senthilkumaran, "Vortex array generation by interference of spherical waves," *Applied Optics*, vol. 46, no. 32, pp. 7862–7867, 2007.

[20] J. Masajada, A. Popiołek-Masajada, and M. Leniec, "Creation of vortex lattices by a wavefront division," *Optics Express*, vol. 15, no. 8, pp. 5196–5207, 2007.

[21] P. Kurzynowski, W. A. Wozniak, and E. Frączek, "Optical vortices generation using the Wollaston compensator," *Applied Optics*, vol. 45, pp. 7898–7903, 2006.

[22] P. Kurzynowski and M. Borwińska, "Generation of vortex-type markers in a one-wave setup," *Applied Optics*, vol. 46, no. 5, pp. 676–679, 2007.

[23] D. P. Ghai, S. Vyas, P. Senthilkumaran, and R. S. Sirohi, "Vortex lattice generation using interferometric techniques based on lateral shearing," *Optics Communications*, vol. 282, no. 14, pp. 2692–2698, 2009.

[24] J. Masajada, "Small-angle rotations measurement using optical vortex interferometer," *Optics Communications*, vol. 239, no. 4–6, pp. 373–381, 2004.

[25] A. Popiołek-Masajada, M. Borwińska, and W. Frączek, "Testing a new method for small-angle rotation measurements with the optical vortex interferometer," *Measurement Science and Technology*, vol. 17, no. 4, pp. 653–658, 2006.

[26] A. Popiołek-Masajada, M. Borwinńska, and B. Dubik, "Reconstruction of a plane wave's tilt and orientation using an optical vortex interferometer," *Optical Engineering*, vol. 46, no. 7, Article ID 073604, 2007.

[27] M. Borwińska, A. Popiołek-Masajada, and P. Kurzynowski, "Measurements of birefringent media properties using optical vortex birefringence compensator," *Applied Optics*, vol. 46, no. 25, pp. 6419–6426, 2007.

[28] M. Santarsiero and R. Borghi, "Measuring spatial coherence by using a reversed-wavefront Young interferometer," *Optics Letters*, vol. 31, no. 7, pp. 861–863, 2006.

[29] J. A. Ferrari and E. M. Frins, "Single-element interferometer," *Optics Communications*, vol. 279, no. 2, pp. 235–239, 2007.

[30] Q. Weijuan, Y. Yingjie, C. O. Choo, and A. Asundi, "Digital holographic microscopy with physical phase compensation," *Optics Letters*, vol. 34, no. 8, pp. 1276–1278, 2009.

[31] M. Takeda, H. Ina, and S. Kobayashi, "Fourier-transform method of fringe-pattern analysis for computer-based topography and inteferometry," *Journal of the Optical Society of America*, vol. 72, no. 1, pp. 156–160, 1982.


Journal of Gravity
Journal of Photonics
The Scientific World Journal
Journal of Soft Matter
Advances in Condensed Matter Physics
Journal of Fluids
Journal of Aerodynamics
International Journal of Statistical Mechanics
International Journal of Optics
Journal of Computational Methods in Physics
Advances in High Energy Physics
Journal of Thermodynamics
Physics Research International
Advances in Astronomy
Journal of Solid State Physics
Journal of Astrophysics
International Journal of Superconductivity
Journal of Biophysics
Journal of Atomic and Molecular Physics